Wireless Power Transmitter for Rare-Earth-Free Wound-Field Synchronous Motors in Hydrogen UAVs

Adrian-Augustin POP
Dept.of Electrical Machines and Drives
Technical University of Cluj-Napoca
Cluj-Napoca, Romania
augustin.pop@emd.utcluj.ro

Ferencz HAVADI
Dept.of Electrical Machines and Drives
Technical University of Cluj-Napoca
Cluj-Napoca, Romania
Havadi.Fe.Ferencz@student.utcluj.ro

Iana POTINGA
Dept.of Electrical Machines and Drives
Technical University of Cluj-Napoca
Cluj-Napoca, Romania
Potinga.Vi.Iana@student.utcluj.ro

***Abstract*— This paper presents a novel modification of a low-power three-phase wound field synchronous motor aimed at improving controllability and efficiency for unmanned aerial vehicle (UAV) propulsion systems. The proposed concept replaces the traditional rotor with a custom wound one that is energized through a wireless power transfer (WPT) system. The stator remains conventionally driven by alternating current, while the rotor functions as a controlled electromagnet powered by rectified wireless energy. The study explores the design, implementation, and evaluation of the wireless excitation system, including resonant coil design, power conversion, and electromagnetic performance. Preliminary results from coil characterization and finite element analysis (FEA) are presented and compared with experimental measurements. The paper concludes with a discussion of system efficiency and outlines future work toward integrated custom transfer coils and optimized magnetic structures via magneto-static analysis. The results demonstrate that the proposed solution provides a compact and efficient excitation method suitable for integration into hydrogen-electric UAV propulsion systems. The approach contributes to improving system reliability, reducing maintenance requirements, and supporting the development of advanced energy-efficient aerial platforms.**

Keywords—resonant circuits, hydrogen fuel cell, inductive coupling, three-phase motor, control systems, wireless power transfer, UAV, finite element analysis, rotor excitation.

I. INTRODUCTION

Hydrogen fuel cell technologies are increasingly considered a key enabler for next-generation UAV propulsion systems demand for efficient and lightweight propulsion systems in unmanned aerial vehicles (UAVs) has led to the widespread adoption of permanent magnet brushless direct-current motors (BLDC) motors due to their high efficiency and power density [1]. Besides great efficiency and excellent power density, these motors also provide limited flexibility in dynamically controlling the rotor magnetic field given their specific topology and construction. Induction squirrel-cage motors on the other hand offer improved robustness and decades of well merited industry appreciation but typically suffer from reduced efficiency at very small mechanical scales [2]. To address these specific limitations, this work proposes a hybrid motor topology where the rotor magnetic field is externally supplied and highly controllable. Wireless power transfer (WPT) provides a viable and robust mechanism for delivering power to rotating or separated systems or mediums without mechanical contact, eliminating the need for brushes or slip rings which are the leading cause of failure of these specific machines [3]. By combining WPT with a wound rotor design, this study introduces a motor concept that allows independent rotor excitation while maintaining mechanical simplicity and the advantages of the permanent magnet synchronous motors (PMSM) robust stator design. Another great safety aspect of the proposed system is the benefit of being able to function in hostile environments where brushed or slip ring designs offer limited running time. Another consideration are mediums in which flammable gases are present, representing a fire risk operating a motor that creates sparks as it functions in case of the Brushed-DC motors or by having worn out slip rings like a traditional wound rotor machine.

II. METHODOLOGY

The utilization of wound-rotor synchronous machines has recently gained traction in UAV propulsion design due to their ability to optimize winding configurations and eliminate rare-earth permanent magnets [4]. The proposed system replaces the conventional wound rotor with a custom wound electromagnet supplied through a resonant inductive transfer system and the respective rectifying circuit. The Stator section remains unmodified during the presented workflow. It generates a rotating magnetic field using a three-phase AC supply at city frequency, while the rotor produces a constant magnetic field through DC excitation. This creates synchronous interaction between the stator and rotor fields enabling angular changes thus torque is generated [5].

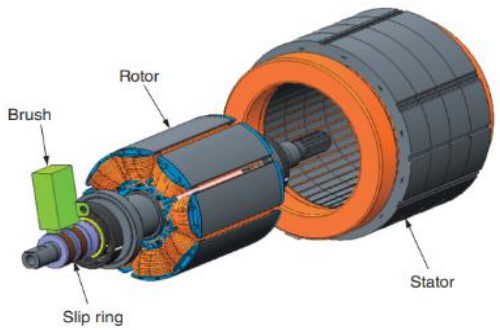

Fig. 1. Topology of the wound rotor machine (reproduced from [9]).

Electrical power is transferred wirelessly to the rotor using inductive coupling between a stationary primary coil and a

This work was supported by a grant co-financed by the European Regional Development Fund, within the Smart Growth, Digitization and Financial Instruments Program 2021-2027, as part of project Romanian Hub for Hydrogen and new energy technologies-Ro-HydroHub, contract no G 2025-113330 din 30.09.2025 to G 2024-81692/390006 from 13.11.2024, SMIS code: 351358.

rotating secondary coil. Both the primary and the secondary coils include a resonant capacitor to maximize energy transfer efficiency operating at their specific resonance frequency [6]. The received AC signal is rectified and filtered to produce a stable DC current for the rotor winding. Wireless Power Transfer efficiency mainly depends on coupling coefficient, alignment, and resonance conditions besides coil quality and the airgap between the coils. Maximum power transfer with minimized reactive losses occurs when both coils operate at the same resonant frequency [7]. On the rotor side, the induced AC voltage is converted into DC using a full-wave rectifier with special low voltage drop diodes to minimize heating and losses, followed by a smoothing capacitor series and noise filtering. This configuration ensures a steady current supply to the electromagnet despite variations in coupling during rotation [8]. Additional smoothing is necessary to minimize electromagnetic interference and destructive switching noise induced by the primary high frequency modulation. The primary coil is powered by a custom small-scale inverter that converts DC voltage into high frequency Pulse width modulated (PWM) alternating voltage that results in a sinusoidal current across the transfer coil given the nature of fast rise/fall times of the supply and the basic inductor behavior to fast changes in voltage in milliseconds. Power is manipulated by altering the duty cycle and the Peak-to-Peak Voltage (V-pp) on the output of the converter while the output of the secondary side will conform by altering its voltage swings and overall waveform shape. Feedback and automation come by measuring the rotors' angular position using strategically placed hall-effect sensors and monitoring the current into the inverter together with the applied voltage at its input side. Another set of hall-effect sensors work in their linear region to characterize the overall strength of the magnetic field around the rotor to establish data for further analyzing the structure to exploit new improvement bases. As a redundant but important safety feature is the temperature that is monitored to give this chain a failsafe operating environment during preliminary testing.

Wireless Power Transfer Coil Driving Circuit

The primary coil is driven using a full-bridge (H-bridge) inverter topology, selected for its ability to generate high-frequency alternating excitation from a low-voltage DC supply. The implemented system operates from a configurable **12–48 V DC** input, enabling flexibility in power scaling and experimental evaluation.

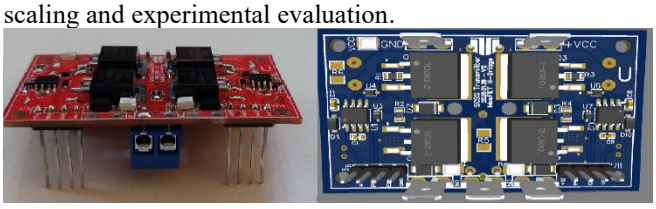

Fig. 2. Efficient H-Bridge package design

The power switching section consists of four N-channel MOSFETs arranged in a full-bridge configuration, driven by two half-bridge gate driver ICs (IR2103 family). This topology enables stable and high bidirectional current flow through the resonant tank, producing an alternating voltage waveform across the primary WPT coil [1]. While measuring only 60x30mm the peak current flow can reach close to 40A while maintaining strong and edge-clean switching. For this reason, we choose to use multilayer PCB to enhance large switching noise suppression and increase the total copper area for minimal resistance both electrically and thermally. Driving high side MOSFETs at **15kHz** frequency requires special attention regarding the bootstrap loop, especially because N-Channel MOSFETs are used in high side switching as well for achieving a higher drive current with minimal power losses. Operating on the high side with N-Channel ones can achieve an order of magnitude lower on state resistance than P-Channel MOSFETs and significantly reduces the bill of material cost of the inverter since these switching components are industry standard on several applications beside specialized operations or niche applications. Achieving similar on state resistance with P Channel semiconductors would certainly be a significant challenge and another important aspect is the symmetry necessary to balance the top and bottom half of the inverter to achieve low noise characteristics. Several combinations of bootstrap capacitors and resistor pairs were tested to find the optimal combo that offers great switching times and low switching losses and current flows into the capacitive gates.

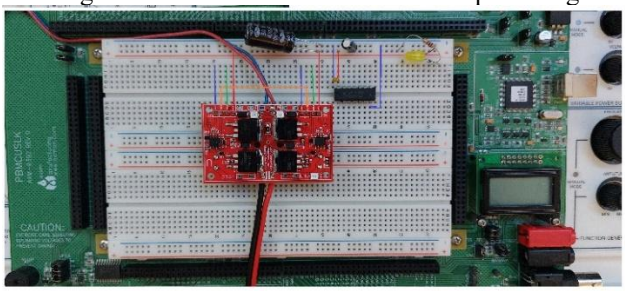

Fig. 3. Initial testing and tuning of the inverter module

To keep the control logic simple the module uses a single PWM signal running on **15 kHz** with voltage domain inside logic level control territory being 0-5V. The signal is inverted using a special high speed SN74 series gate array to build the complementary part for the other side of the bridge in real time with no digital processor needed to calculate two different signals at one. Through this hardware choice we eliminated the expensive microcontroller-based development board being able to use a single channel precision function generator. The National Instruments Elvis2+ model shown in Fig. 4. served a major role in the testing phase, offering great user interfaces and excellent hardware packages. This approach ensures proper half-bridge operation while maintaining tight timing control between switching devices. Such complementary drive schemes are commonly used in resonant and high-frequency inverter systems to minimize cross-conduction and switching losses.

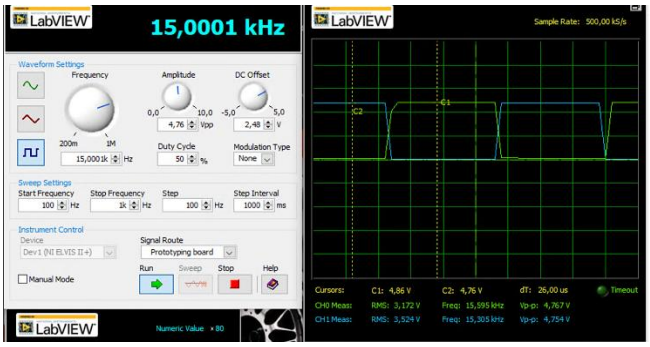

Fig. 4. Experimental setup for generating the control and the complementary signal of the inverter

A shared enable (EN/COM) control line is implemented across both driver stages, allowing synchronized activation and rapid shutdown capability for the entire bridge increase its practicality and energy requirements. The separation between the main power supply (12–48 V) and the bootstrap supply improves reliability and ensures consistent gate overdrive voltage under varying load conditions. Proper bootstrap design is critical in high-frequency applications to maintain switching efficiency and prevent partial MOSFET turn-on. A key feature of the design is the integration of the resonant compensation network directly within the H-bridge stage. The primary coil is paired with a high-frequency MKP film capacitor (MKP1G031504F00JSSD), forming a series or parallel resonant circuit depending on configuration. By tuning the resonant frequency to match the secondary coil network, the system achieves enhanced coupling and maximized energy transfer. Despite these challenges, topology provides a suitable platform for driving resonant WPT systems and allows easy integration with control electronics.

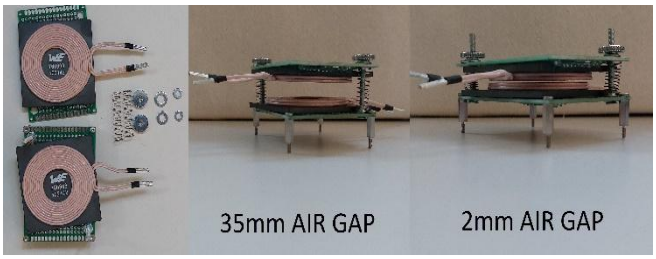

Fig. 5. Experimental test stand for adjustable air gap

The wireless power transfer (WPT) system utilizes a pair of identical commercially available coils (Würth Elektronik), selected for their high-power handling capability and integrated ferrite shielding. These coils are rated for power levels up to 200 W, making them suitable for validating the proposed rotor excitation approach under realistic operating conditions. Presented solution fits perfectly and satisfies all requirements imposed by the generation characteristics of the setup. The springs provide a controlled outward force, ensuring stable mechanical positioning while allowing precise adjustment of the air gap between the coils using the threaded rods. Preliminary simulations and testing show that the screws and the spring do not cause unwanted influence over the magnetic fields and their presence can be negated. As visible in the setup, the coils remain coaxially aligned while the vertical spacing can be varied continuously. Each coil is paired with a compensation capacitor to form a resonant tank. The system operates under resonant inductive coupling, where maximum power transfer occurs when both primary and secondary circuits are tuned to the same frequency-f_0 where L is the inductance of the coil and C the compensation formula as shown in formula (1).

$$f_0 = \frac{1}{2\pi\sqrt{LC}} \quad (1)$$

Despite these challenges, the ability to transfer substantial power levels without physical contact demonstrates the feasibility of using WPT for rotor excitation. With the resonance nailed, future steps include custom PCB-based coils, enabling precise geometry control and reduced thickness, optimized ferrite backings, designed specifically for motor geometry and coil designs tailored for rotational misalignment tolerance.

On the secondary side of the wireless power transfer system, the received high-frequency AC signal must be converted into a stable DC supply to energize the rotor coil. Voltage induced in the secondary coil is rectified using a full-wave Schottky diode bridge. Schottky diodes were selected due to their low forward voltage drop, minimizing conduction losses; fast switching characteristics, enabling efficient operation at high frequencies; and high current handling capability, required for elevated power levels. Compared to conventional PN junction diodes, Schottky devices exhibit negligible reverse recovery time, which significantly reduces switching losses and improves overall system efficiency in resonant WPT applications [8]. Following rectification, a smoothing capacitor is used to reduce voltage ripple and provide a stable DC output suitable for energizing the rotor winding.

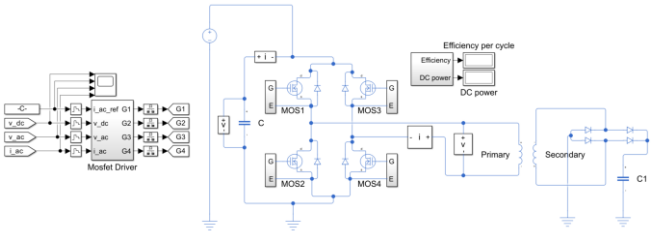

Fig. 6. Inverter and wireless power transfer diagram

To accurately evaluate the power transfer capability of the WPT system independently of the rotor, a custom-designed constant power electronic load was developed. By adjusting the load parameters, the system can simulate different rotor excitation scenarios, enabling detailed analysis of WPT performance without requiring continuous motor operation.

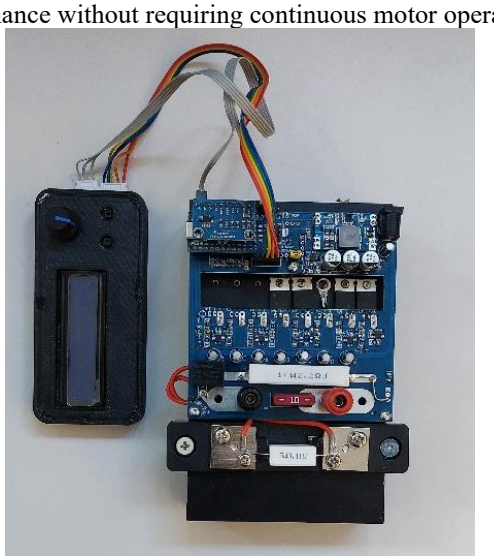

Fig. 7. High current programmable load

An important feature of the developed constant power load is its ability to emulate not only the static electrical characteristics of the rotor winding, but also its dynamic interaction with the stator magnetic field. In an actual machine, the effective electrical behavior of the rotor is not purely resistive. Instead, it varies depending on the

electromagnetic interaction between the rotor and the stator's rotating magnetic field. This interaction influences the current distribution and can be interpreted as a dynamic change in the equivalent impedance of the rotor winding. By incorporating this dynamic adjustment, the test setup more accurately represents the conditions encountered in the actual motor system, where the rotor excitation is influenced by both the supplied DC current and the stator-induced electromagnetic forces.

III. ELECTROMAGNETIC FINITE ELEMENT ANALYSIS

To validate the electromagnetic behavior of the wireless power transfer system and evaluate the magnetic field distribution, a finite element method (FEM) simulation was performed using the Finite Element Method Magnetics (FEMM) software package. Given the structure of the system, a 2D axisymmetric problem formulation was selected. This approach harnesses the rotational symmetry of the circular coils around the central vertical axis (r=0), reducing computational expense while maintaining physical precision, compared to 3D models. The simulation domain was restricted using an asymptotic boundary condition to emulate an infinite open space. The mesh was refined dynamically, particularly within the multi-strand copper conductor and the ferrite shielding layer, where high gradients of magnetic lux density are expected. The material properties were defined: the copper windings were modeled with relative permeability μ_r= 1 and the electrical conductivity σ=1 MS/m, individual turns were grouped as a circuit property to enforce uniform current distribution; the shielding layer was assigned a ferrite material model with high initial relative permeability ($\mu_r = 2000$) and electrical conductivity of σ = 2000; the surrounding medium was defined as Air with $\mu_r = 1$; intensity I = 30 A.

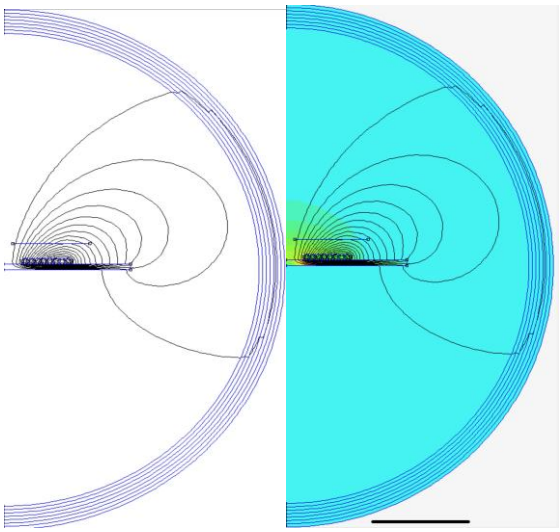

Fig. 8. Magnetic vector potential lines showing the flux paths.

The prominent magenta zone on the left boundary appears because of the model's symmetry. Since r = 0 represents the central axis of rotational symmetry, the other half of the circular coil is mathematically mirrored on the opposite side. This peak intensity represents the physical point where both magnetic fields of both halves of the circular coil meet. Moving outward from the central axis if symmetry, the scalar color mapping displays a controlled distribution of the magnetic flux density (B). The green zones located immediately around the copper turns, capture the highest concentration if the magnetic field generated by the 30 A current. As the distance from the coil increases, the color shifts towards the blue spectrum, indicating that the magnetic flux naturally dissipates and reaches zero in the far field. A key element in this distribution is the soft ferrite backing plate. Due to the material having a high relative magnetic permeability, the magnetic vector potential lines are tightly confined inside the ferrite layer. By trapping the magnetic flux, the ferrite shield performs two critical functions for the UAV system. First, it ensures that the magnetic field is directed entirely toward the drone's receiver, thus maximizing flux linkage and keeping transmission efficient at 15KHz. Second, it eliminates arbitrary magnetic fields behind the transmitter, preventing electromagnetic interference from disturbing the electronics, compass modules or flight controllers on the drone during landing.

To verify the mathematical consistency of the 2D axisymmetric finite element model, the global parameters computed at a current of ***30 A*** and the operating frequency of ***15 kHz***. *Calculating self-inductance using the following formula:*

$$L = \frac{Flux}{Current} = 5.36195 * 10^{-6} \quad (2)$$

To extract the exact magnetic flux linkage circulating through system boundaries when the excitation parameters are configured for a total input of I = 30A, the fundamental flux linkage formulation must be applied:

$$\lambda_{simulated} = \frac{Flux}{Current} * I \quad (3)$$

Where: $\lambda_{simulated} = 1.608585 * 10^{-4}\, Wbcu.$

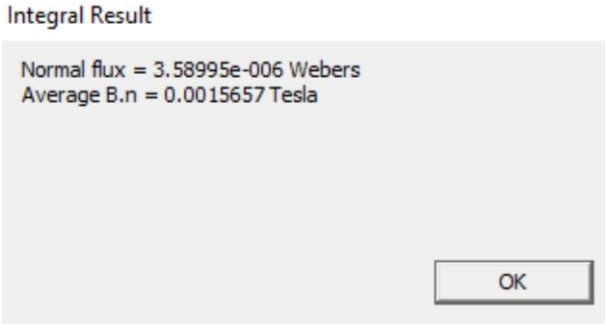

Fig. 9. Computed normal magnetic flux and average induction

To confirm that the 2D geometric model replicates physical conditions with precision, the flux matrix is benchmarked directly against the official factory technical sheet of the Würth Elektronik 76039102142 coil. The manufacturer specifies a nominal self-inductance of $L_{nominal} = 5.30\ \mu H$ for the physical component. At the target operational current of 30 A, the ideal theoretical flux linkage expected withing a flawless system is determined by the following relationship:

$$\lambda_{official} = L_{nominal} * I \quad (4)$$

$$\lambda_{official} = 5.30 * 10^{-6} * 30A = 1.5900 * 10^{-4} Wb$$

The relative percentage error is calculated using the standard deviation formulation:

$$\epsilon = \left|(\lambda_{simulated} - \lambda_{official})/\lambda_{official}\right| * 100\% \quad (5)$$

$$\epsilon = 1.168\%$$

After multiple numerical testing and systematically moving the top evaluation boundary line across spatial coordinates, we have concluded the following behaviors: First, by moving the integration boundary from a proximal of 2mm to a maximum displacement of 10mm from the physical copper windings, the numerical engine records a progressive stabilization of the average induction, proving that the near-field electromagnetic interactions transition smoothly into a predictable far-field dissipation zone. Second, these consecutive tests prove that the geometry of the transmitter is highly optimized for spatial tolerances. Even after simulating the worst-case landing misalignments, the core magnetic properties do not suffer from disastrous field degradation or uncompensated leakage paths.

IV. RESULTS AND DISCUSSION

The wireless power transfer system was experimentally characterized by maintaining a constant output power of 200 W on the secondary side while varying the air gap between the primary and secondary coils. The input power required to sustain this output was measured, allowing calculation of the overall system efficiency as a function of coil separation. As shown in Fig. 10, the output power remains constant at 200 W across all measured distances, while the required input power increases with increasing air gap. At minimal separation (0–5 mm), the input power is approximately 203–204 W, corresponding to an efficiency close to 98–99%. This trend clearly illustrates the expected degradation in efficiency due to reduced magnetic coupling between the coils. As the air gap increases, the coupling coefficient decreases, requiring higher primary-side current and increased input power to maintain the same output level [10]. The calculated efficiency decreases almost linearly over the tested range, dropping from approximately 98.5% at small gaps to roughly 93% at the largest tested distance. This reduction is primarily attributed to increased leakage flux, reduced mutual inductance and higher reactive power in the resonant network.

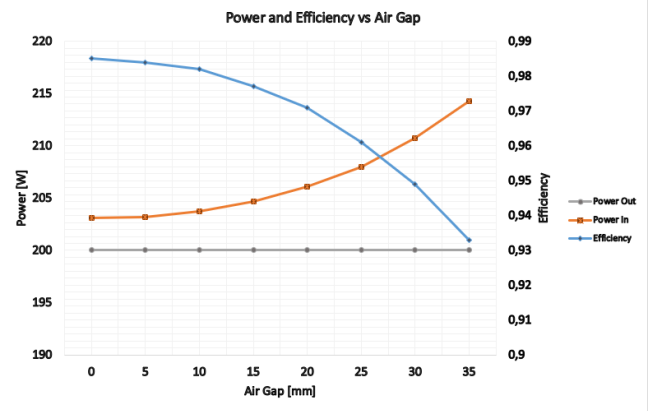

Fig. 10. Experimental results: Power and efficiency vs air gap

Although maximum efficiency is achieved at minimal separation, practical considerations introduce additional constraints. Thermal management becomes increasingly important at higher power levels. The experimental data aligns well with theoretical predictions and simulation results, confirming the strong dependence of system efficiency on coupling conditions. The identification of a balanced operating point at approximately **5 mm** is therefore a key outcome of this study, demonstrating that high efficiency can be maintained without compromising system reliability or cooling performance.

The FEA simulation confirms that the model matches the physical commercial coil, yielding similar results to the manufacturer's official datasheet values. After generating multiple simulations, the error margin was excellent at just 1.16%, confirming that the model is highly accurate. Finally, the parametric gap tests fully validate the physical setup as stable and optimized.

The next phase of research will integrate a lightweight Hydrogen Proton Exchange Membrane Fuel Cell (PEMFC) fed by a solid-state, rare-earth hydrogen storage reservoir, Fig. 11. This specialized reservoir will utilize rare-earth metal hydrides to achieve high-density, low-pressure hydrogen storage, drastically improving volumetric efficiency and safety compared to conventional high-pressure tanks. To manage the overall power distribution, this fuel cell network will be paired with a high-power-density battery booster pack via a bidirectional DC-DC converter, effectively handling peak power demands and rapid transient responses during aggressive flight maneuvers. The control algorithms developed in this work will be migrated to a low-footprint microcontroller to execute high-frequency, sensorless field-oriented control, thereby eliminating heavy position sensors and minimizing the physical footprint of the Electronic Speed Controller (ESC).



Fig. 11. Experimental test bench layout of the hydrogen PEM fuel cell and iEESM powertrain system for heavy-load UAV applications

V. CONCLUSIONS

This work proposes a hybrid motor topology suitable for integration into hydrogen-electric UAV propulsion systems using a novel approach for rotor excitation in small-scale electric machines by combining a conventional three-phase stator with a wirelessly powered wound rotor. By replacing the traditional wound rotor with an externally energized electromagnet, the proposed system enables independent control of the rotor magnetic field while maintaining a contactless and mechanically simple architecture. A key contribution of this study is the successful integration of a resonant wireless power transfer (WPT) system capable of

delivering power levels up to 200 W, demonstrating the feasibility of supplying sufficient energy for rotor excitation without the use of slip rings or brushes. The use of a high-frequency H-bridge inverter, resonant compensation, and optimized coil selection enabled efficient operation under varying conditions.

Experimental characterization confirmed that system performance is strongly dependent on coil alignment and air gap. With a constant output power of 200 W, efficiency remained high (>98%) at small separations and decreased gradually with increasing distance, reaching approximately 93% at the maximum tested gap. An air gap of approximately 5 mm was identified as an optimal operating point, providing an effective compromise between high efficiency and improved thermal management, which is critical for continuous operation. The experimental results were supported and validated through magnetic finite element simulations, showing strong agreement in observed trends and system behavior. This correlation confirms the reliability of the proposed design and the effectiveness of the modeling approach in predicting real-world performance.

REFERENCES

[1] J. Smith, “Brushless DC motor efficiency in UAV applications,” IEEE Trans. Ind. Electron., 2020.

[2] A. Kumar, “Performance limitations of small induction motors,” IET Electric Power Applications, 2019.

[3] S. Li and C. Mi, “Wireless power transfer for electric systems,” IEEE Journal, 2015.

[4] Kim, S.-E.; You, Y.-M. Wound-Rotor Synchronous Motor with Toroidal Windings for UAV Propulsion Systems. *Actuators* 2026, *15*, 82. https://doi.org/10.3390/act15020082

[5] P. Vas, “Synchronous Machine Theory,” Oxford Press, 1992.

[6] A. Kurs et al., “Wireless power transfer via strongly coupled resonances,” Science, 2007.

[7] B. L. Cannon, “Resonant inductive coupling design,” IEEE Trans. Power Electronics, 2009.

[8] M. K. Kazimierczuk, “RF Power Amplifiers,” Wiley, 2008.

[9] S. Sakurai and T. Suwazono, “EV Traction Wound Field Synchronous Motor,” MEIDEN Review, Series No. 182, no. 2, pp. 34.2021.

[10] Elnail, K. E. I., Huang, X., Xiao, C., Tan, L., & Haozhe, X. (2018). Core structure and electromagnetic field evaluation in WPT systems for charging electric vehicles. *Energies*, *11*(7), 1734. https://doi.org/10.3390/en11071734